

# Quantum Dynamical Rate Constant for the H + O<sub>3</sub> Reaction Using a Six-Dimensional Double Many-Body Expansion Potential Energy Surface Revisited

H. Szichman,<sup>†</sup> M. Baer,<sup>‡</sup> and A. J. C. Varandas<sup>\*,†</sup>

*Departamento de Química, Universidade de Coimbra, P-3049 Coimbra Codex, Portugal, and Department of Physics and Applied Mathematics, Soreq NRC, Yavne 81800, Israel*

*Received: June 1, 1998; In Final Form: August 5, 1998*

New quantum dynamics computations of the rate constant for the atmospheric reaction  $\text{H} + \text{O}_3 \rightarrow \text{O}_2 + \text{OH}$  are reported. These calculations have been carried out under the assumption of an atom-to-atom reactive process scheme rather than on the basis of the global atom–molecule reactive scattering approach reported in a previous paper by the same authors (*J. Phys. Chem.* **1997**, *101*, 8817). Agreement with the available classical trajectory results are now notably improved, although the new theoretical results still continue to agree best with the more recent experimental data of Clyne and Monkhouse and Greenblatt and Wiesenfeld for the title reaction.

## 1. Introduction

The chain-branching  $\text{H} + \text{O}_3$  reaction plays a key role in atmospheric chemistry, and hence the high interest and research, both experimental<sup>1–18</sup> and theoretical,<sup>19–21</sup> on such a reaction come as no surprise.

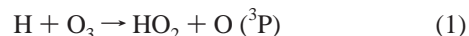
Contributing to this trend of better understanding its mechanism, the present authors have recently published a paper<sup>21</sup> presenting the first quantum mechanical (QM), three-dimensional (3D), infinite-order-sudden-approximation (IOSA) study of the title reaction, using a previously reported double many-body expansion (DMBE)<sup>22</sup> potential energy surface<sup>19</sup> for ground-state HO<sub>3</sub>. The computed cross sections and rate constant<sup>21</sup> were then found in moderate agreement with both the recommended experimental data<sup>23</sup> and the available quasiclassical trajectory (QCT) results.<sup>19,20</sup> Although appreciable differences between the QCT and QM results have been noted in the past,<sup>24,25</sup> particularly near the threshold energy, it is somewhat disturbing that in a process like  $\text{H} + \text{O}_3 \rightarrow \text{HO} + \text{O}_2$ , where the presence of an hydrogen atom would imply the existence of significant quantum-mechanical effects, the calculated results indicate that the QCT predictions fell much closer to the recommended experimental data<sup>23</sup> than the QM ones. Although some of the discrepancy between theory and experiment can be ascribed to inaccuracies of the HO<sub>3</sub> potential energy surface, this matter should be of no concern for the classical vs quantum comparison reported in that paper, since both calculations have been based on the same surface. In this paper we focus our attention on the relatively large scatter of the experimental results and on the so-called zero-point energy (ZPE) leakage (we give here some recent papers<sup>26–32</sup> on this topic from which others may be obtained by cross-referencing), which have also been claimed to contribute to the issues discussed in ref 21 (hereafter referred to as paper I).

In the next section, an explanation is given of how a new reactive approach may be adopted within the 3D quantum mechanical scattering model reported in paper I, which allows a better estimate of the reactive probabilities for the title reaction.

In sections 3 and 4, the revised results are presented and further discussed. The conclusions are in section 5.

## 2. The Atom-to-Atom Reaction Mechanism

As in paper I, the quantum dynamics approach used to determine the reactive probabilities is based on the calculation of all nonreactive probabilities, i.e.,  $P(t \leftarrow t_0)$ , the sum of which is then subtracted from unity. Notably, this method has the advantage of avoiding detailed state-to-state reactive probability calculations, which would be prohibitive for the title system. Of course, such a procedure is hopeless if one wishes to discriminate the states in the products. Moreover, assumptions have to be made in order to interpret the computed results. For example, in paper I we have assumed that, in agreement with the suggestions of the majority of the experimental authors,<sup>1,3,17,18</sup> most of the available energy in the title reaction would be released to form  $\text{HO} + \text{O}_2$  products. The loss of reactive probability due to the presence of the alternative reaction channel



first proposed by Finlayson-Pitts and Kleindienst<sup>11</sup> has therefore been neglected, since in some later experimental work undertaken by the same group<sup>12</sup> and Washida et al.<sup>10</sup> it has been suggested that reaction 1 could attain ca. 3–6% of the overall reaction of H with O<sub>3</sub>. Furthermore, previous QCT studies<sup>19</sup> corroborate the fact that reaction 1 should have little significance for the calculations being carried out in the present work over the range 0–0.5 eV. More difficult is the implicit assumption made in paper I that the H atom could attack with equal probability each of the oxygen atoms forming the ozone molecule<sup>20</sup> owing to its 3-fold permutational symmetry. This attribute is built into the DMBE HO<sub>3</sub> potential energy surface,<sup>22,33</sup> which is symmetrical under permutation of the three oxygen atoms. In a retrospective analysis of the results obtained in paper I, we may question whether this last condition has been properly fulfilled, when a reduced dimensionality 3D IOSA QM calculation is applied to study the title reaction using the HO<sub>3</sub> DMBE potential energy surface. Indeed, we have already

<sup>†</sup> Universidade de Coimbra.

<sup>‡</sup> Soreq NRC.

pointed out in paper I the difficulties encountered in implementing such an assumption. It was then noted that when the hydrogen atom attacks the central oxygen atom of the ozone molecule, a very high barrier must be overcome for the  $\text{H} + \text{O}_3$  reaction to take place. At this point it is convenient to recall the Jacobi coordinate system used in paper I to describe both arrangement channels of the four-atom system, as illustrated in Figure 2 of the same paper. Thus, the atom–triatom (reagent) channel is described there by three radial distances and three Jacobi angles. The former include the vibrational coordinate  $r$  for one of the extreme bonds presumed to be the “stronger” one (later assumed to be unbreakable), the corresponding translational coordinate of the triatom  $\rho$  connecting the third atom with the center of mass of the “stronger” bond, and the translational coordinate  $R$  which connects the fourth atom to the center of mass of the triatomic system. Three Jacobi angles complete the description of the system:  $\theta$  (the angle between  $r$  and  $\rho$ ),  $\gamma$  (the angle between  $\rho$  and  $R$ ), and  $\beta$  (the polar angle between the triatom plane and  $R$ ). Returning to the above-mentioned question of the very high barrier that must be overcome, the meaning of this fact is that the analysis of this reaction using a 3D bimolecular QM collisional method will not essentially include reactive probabilities between the attacking H and the central O atom for most of the chosen IOSA  $\gamma$  directions and range of energies of interest to calculate the rate constant near room temperature. Additionally, by examining Figure 4 of paper I, which shows the angular distribution of the total cross section as a function of the angle  $\gamma$ , one is led to conclude that the extreme oxygen atoms are not attacked symmetrically in contradiction with the potential energy surface permutational symmetry. This last effect may be attributed to fact of having used an atom–diatom configuration scheme<sup>34,35</sup> for representing the ozone molecule. Such a scheme is of general applicability,<sup>35</sup> although it may be not be optimum to describe the full symmetry that is present in  $\text{A}_3$  systems such as ozone. Certainly, the above discussion is irrelevant if a full dimensional analysis were used to study the  $\text{H} + \text{O}_3$  reactive process. Since this approach is outside the present computing capabilities, we have been motivated to look for a better approximation within the 3D IOSA model.

From the above discussion, one can infer that the previous published results<sup>21</sup> may be affected by a factor varying between  $3/2$  and 3, depending on the true number of oxygen atoms that intervene in the reaction with H. To elucidate this point, within the framework of the present QM model, we have devised a better approach to the problem. We suggest to return to the scheme already successfully used for studying the  $\text{O}_4$ <sup>36</sup> and  $\text{HHOH}$ <sup>24,25</sup> systems. In these publications one of the bonds (the diatom in the atom–diatom configuration) has been assumed to be stronger than the others and hence considered unbreakable (“spectator”) during the reactive process. Thus, in the present case we are allowed to multiply the results obtained for a single isomeric structure of the reactant ozone molecule by a factor of 3, since there are three equivalent such isomeric structures. To achieve this goal, given the symmetry properties of the  $\text{HO}_3$  DMBE potential energy surface,<sup>19</sup> one could simply “freeze” the stretching distance of one of the  $\text{O}_2$  bonds, ensuring in this way that only the third O atom can react. This type of procedure, which has already been tested in the past,<sup>37,38</sup> may nevertheless introduce artifacts in the computed results<sup>39</sup> and overestimate (underestimate) the reaction probabilities. This can be understood from the fact that we do not allow the energy to be spent in exciting the vibrational modes of the unbroken bond without leading forcibly to (or inhibiting) reaction. We

**TABLE 1: Vibrational States of Ozone in eV**

state <sup>a</sup>	this work	ref 41	exptl ref 42
(000)	0	0	0
(010)	0.083	0.082 77	0.086 90
(001)	0.130	0.130 33	0.129 20
(100)	0.132	0.132 26	0.136 77
(020)	0.162	0.163 05	0.173 49
(011)	0.208	0.210 00	0.214 06
(110)	0.210	0.211 08	0.222 59
(030)	0.241	0.242 57	0.255 26

<sup>a</sup> We use the common spectroscopic notation ( $n_1, n_2, n_3$ ) where  $n_1$ ,  $n_2$ , and  $n_3$  indicate the quantum numbers for symmetric stretching, bending, and asymmetric stretching.

have then adopted a milder restriction by eliminating the absorbing negative imaginary potential (NIP)<sup>40</sup> along the assumed unbroken  $\text{O}_2$  bond while reducing its vibrational amplitude limits ( $r$ ) and extending it for the distance  $\rho$ . With this approach, we may reasonably expect that most of the reactive probabilities can be ascribed only to one of the terminal O atoms in  $\text{O}_3$ .

### 3. Results and Discussion

To stress that the problems in the results presented in paper I have been eventually due to reduced dimensionality effects rather than to the present 3D IOSA QM model itself, we compare in Table 1 the seven lowest computed energy levels of the  $\text{O}_3$  molecule using the present atom–diatom scheme<sup>35</sup> with other available theoretical results<sup>41</sup> and the experimental ones.<sup>42</sup> Clearly, the differences between the theoretical and experimental values are due to inaccuracies of the  $\text{O}_3$  potential energy surface in the vicinity of the potential well. More significant, however, is the agreement between the two sets of theoretical results, which may be considered as good for the purposes of the present work.

The main issue of the present paper is therefore to define a new NIP expression

$$V_1(r, R) \equiv i[\nu_{\text{tr}}(r) + \nu_{\text{IR}}(R)] \quad (2)$$

where only a vibrational term,  $i\nu_{\text{tr}}(r)$ , and a translational one,  $i\nu_{\text{IR}}(R)$ , are taken into account ( $R$  is the distance connecting the position of the H atom and the center of mass of the ozone molecule; all coordinates are defined as in Figure 1 of paper I). For other details concerning the present QM model, the reader is also referred to paper I.

In the present work, reactive probabilities were computed for translational energies  $E_{\text{tr}}$  ranging from 0.05 to 0.40 eV, which are relevant for the calculation of the rate constant near room temperature. The contribution of higher energies were estimated by fitting an analytical expression to the computed cross sections (see later). In fact, the explicit calculation of cross sections for the title reaction at much higher translational energies would simply be unaffordable given the present computing availabilities. Besides, a reduced dimensionality 3D IOSA scheme becomes inadequate to analyze accurately such high values of  $E_{\text{tr}}$ . This is due to the rotational contributions that may become very important when describing the mechanisms for energy dissipation during the reactive process. Figure 1 shows the new calculated reactive probabilities for the title reaction as a function of the total angular momentum. The results are then presented for above-mentioned translational energies  $E_{\text{tr}}$  ranging from 0.05 to 0.40 eV at intervals of 0.05 eV. As in paper I, the distributions show in all cases a maximum at  $J = 0$  decreasing

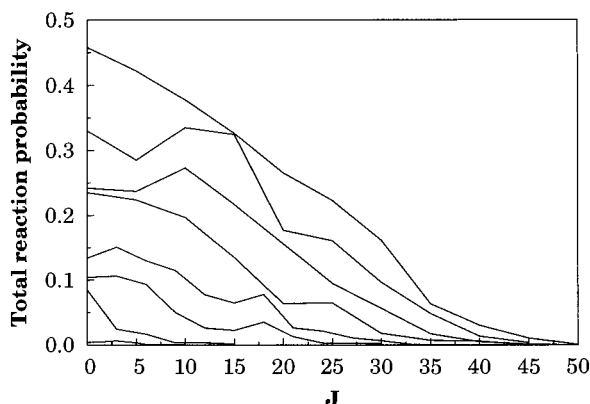


**Figure 1.** Opacity functions calculated as a function of the total angular momentum. Curves have been computed for values of  $E_{tr}$  ranging from 0.05 to 0.40 eV in steps of 0.05 eV, which can be identified in ascending order by going from bottom to top at  $J = 0$ .

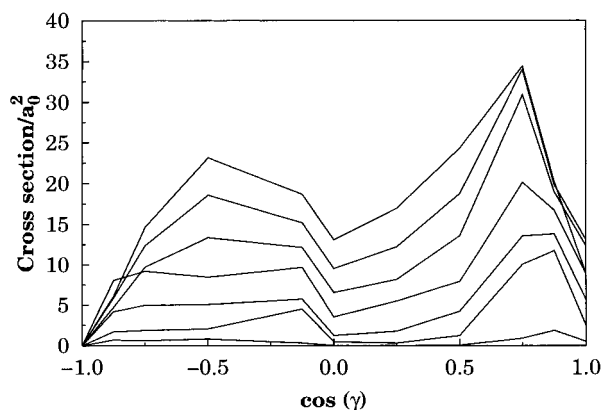


**Figure 2.** Angular distribution of total cross sections as a function of the angle  $\gamma$ . Curves are shown for the same cross translational energies as in Figure 1 and can be identified for increasing values of  $E_{tr}$  by going from bottom to top at  $\cos(\gamma) \sim -0.25$ .

to zero at a cutoff  $J$  value, which increases with increasing energy. Figure 2 presents the  $\gamma$ -dependent cross sections. The observed asymmetry with respect to the angle  $\gamma$  is now expected since the model discriminates between the terminal O atoms of ozone. We also note that we may have led the reader in paper I to think that the peak at  $\gamma = 120^\circ$  is due only to the attack of H on the second terminal atom of ozone (which corresponds to the unbroken bond in the present work). This might be true only for a coplanar configuration of the reactive process, which is clearly not the case in our 3D calculations. (Parenthetically, we note that even for the coplanar case, quantum mechanics might allow some reactivity, no matter how small it might be.) In fact, both in the present work and in paper I, the following 5D polar angle averaged potential energy surface has been used for the reactant arrangement channel

$$\bar{U}(r\rho R\theta\gamma) = \frac{1}{\pi} \int_0^\pi \bar{U}(r\rho R\theta\gamma\beta) d\beta \quad (3)$$

where all symbols have the meaning previously assigned. Thus, the cross sections shown in Figure 2 are the result of averaging the reactive probabilities over all polar directions, besides the coplanar case ( $\beta = 0$ ). Consequently, the peak at  $\gamma = 120^\circ$  may also include important contributions due to the reaction between H and the first terminal O atom of ozone.

In Table 2 and Figure 3 we show the reactive cross section as a function of the translational energy. This has been fitted

**TABLE 2: Numerical Values of the Reactive Cross Sections Calculated in the Present Work<sup>a</sup>**

$E_{tr}/\text{eV}$	$\sigma^r/a_0^2$	$E_{tr}/\text{eV}$	$\sigma^r/a_0^2$
0.05	0.09	0.25	9.12
0.10	0.50	0.30	12.6
0.15	3.16	0.35	15.9
0.20	5.42	0.40	18.9

<sup>a</sup> For a comparison with other theoretical results, see Figure 2.

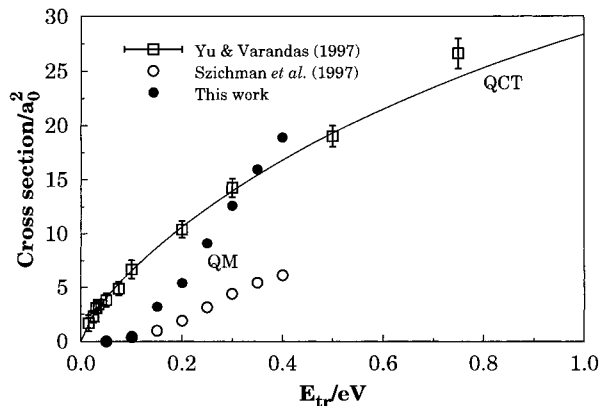


**Figure 3.** Cross section as a function of translational energy for the process  $\text{H} + \text{O}_3 \rightarrow \text{HO} + \text{O}_2$ . A comparison between QM and QCT is shown. The full line indicates the fit to the actual QCT results, which are indicated by the open squares; also shown are the corresponding error bars. This QM results from the present work are indicated by the solid dots, and the previous results<sup>21</sup> by open ones.

to the same analytical form as in paper I

$$\sigma^r = CE^n \exp(mE) \quad (4)$$

where the parameters  $C = 8.30$ ,  $n = 0.5$ , and  $m = 3.27$  are given in units such that with  $E$  in eV the cross section is given in  $a_0^2$ . Of course, no attempt has been made to obtain a proper description of the antithreshold behavior, i.e.,  $\sigma^r \rightarrow 0$  at very high collisional energies. This should have no effect on the calculations reported in the present work. Equation 4 has then been used to calculate the thermal rate coefficient in the usual way. It leads to the exact form<sup>20,43</sup>

$$k(T) = C \left( \frac{8k_B T}{\pi\mu} \right)^{1/2} \frac{(k_B T)^n \Gamma(n+2)}{(1 - mk_B T)^{n+2}} \quad (5)$$

where  $k_B$  is the Boltzmann constant and  $\mu$  is the atom-triatom reduced mass. The calculated rate constant is shown graphically in Figure 4 as a function of temperature. In addition to the results obtained with the new approach, we give for comparison in Figure 3 and Figure 4 the old QM calculations<sup>21</sup> and the QCT ones.<sup>19</sup> For completeness, the available experimental estimates are also indicated in Figure 4. As it is seen, the QM vs QCT agreement has been considerably improved with respect to results reported in paper I. The fact that the major disagreement occurs near the threshold energy for reaction, where the QCT results clearly overestimate the QM ones, suggests that ZPE leakage may be an important source of error as indeed found on other previous occasions.<sup>25,44</sup> Of course, the possibility that the dynamical constraints in the QM method underestimate the reaction probability at low energies cannot also be ruled out. From the experimental point of view, the agreement with our QM results is as before<sup>21</sup> best with the results of Clyne and Monkhouse<sup>5</sup> and the more recent data by Greenblatt and Wiesenfeld.<sup>8</sup>

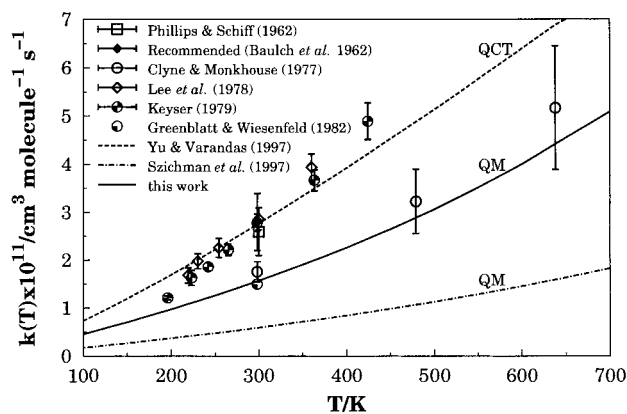


**Figure 4.** Linear plot of the rate constant as a function of  $T$ : full line, this work QM results; dash-dot line, previous QM results;<sup>21</sup> dashed line, QCT results. Experimental results are taken from refs 4–8. The recommended value of ref 23 is shown by the solid diamond.

#### 4. Conclusions

We have carried out 3D QM calculations of the reaction  $\text{H} + \text{O}_3 \rightarrow \text{HO} + \text{O}_2$  using an atom-to-atom reaction process scheme (rather than a global atom-molecule collisional approach employed in paper I) in order to diminish the effects due to reduced dimensionality. The new quantum dynamical computations of the cross sections and rate constant have been compared with QCT calculations based on the same  $\text{HO}_3$  DMBE potential energy surface. The agreement with the QCT results is now notably improved, although the latter still overestimate considerably the QM ones near the threshold energy for reaction, a fact that has partly been attributed to zero-point energy effects. Thus, it would be interesting to assess their importance as previously done, e.g., for the  $\text{H} + \text{O}_2$  reaction.<sup>45</sup> Moreover, the new theoretical computations continue to support the last experimental data obtained for the title reaction by Clyne and Monkhouse,<sup>5</sup> and more recently by Greenblatt and Wiesenfeld.<sup>8</sup> Finally, we note that the removal of the NIP potential previously<sup>21</sup> located in the one of the  $\text{O}_2$  bonds of ozone leads essentially to the same value of reactivity as in paper I. This corroborates the fact that one of the two  $\text{O}_2$  bonds acts as “spectator” during the reactive collisional process, in agreement with the trajectory results reported elsewhere.<sup>20</sup>

**Acknowledgment.** This work has the support of Fundação para a Ciência e Tecnologia, Portugal, under programs PRAXIS XXI and FEDER (Contract 2/2.1/QUI/408/94).

#### References and Notes

(1) Charters, P. E.; Macdonald, R. G.; Polanyi, J. C. *Appl. Opt.* **1971**, *10*, 1747.

- (2) Anlauf, K. G.; Macdonald, R. G.; Polanyi, J. C. *Chem. Phys. Lett.* **1968**, *1*, 619.
- (3) Polanyi, J. C.; Sloan, J. J. *Int. J. Chem. Kinet. Symp.* **1975**, *1*, 51.
- (4) Keyser, L. F. *J. Phys. Chem.* **1979**, *83*, 645.
- (5) Clyne, M. A. A.; Monkhouse, P. B. *J. Chem. Soc., Faraday Trans. 2* **1977**, *73*, 298.
- (6) Phillips, L. F.; Schiff, H. I. *J. Chem. Phys.* **1962**, *37*, 1233.
- (7) Lee, J. H.; Michael, J. V.; Payne, W. A.; Stief, L. J. *J. Chem. Phys.* **1978**, *69*, 350.
- (8) Greenblatt, G. D.; Wiesenfeld, J. R. *J. Geophys. Res.* **1982**, *87*, 11145.
- (9) Finlayson-Pitts, B. J.; Kleindienst, T. E.; Ezell, M. J.; Toohey, D. *W. J. Chem. Phys.* **1981**, *74*, 4533.
- (10) Washida, N.; Akimoto, H.; Okuda, M. *J. Chem. Phys.* **1980**, *72*, 5781.
- (11) Finlayson-Pitts, B. J.; Kleindienst, T. E. *J. Chem. Phys.* **1979**, *70*, 4804.
- (12) Howard, C. J.; Finlayson, B. J. *J. Chem. Phys.* **1980**, *72*, 3842.
- (13) Force, A. P.; Wiesenfeld, J. R. *J. Chem. Phys.* **1981**, *74*, 1718.
- (14) Bates, D. R.; Nicolet, M. *J. Geophys. Res.* **1950**, *55*, 301.
- (15) Herzberg, G. *J. R. Astron. Soc. Canada* **1951**, *45*, 100.
- (16) Meinel, A. B. *Astrophys. J.* **1950**, *112*, 120.
- (17) Ohoyama, H.; Kasai, T.; Yoshimura, Y.; Kuwata, H. *Chem. Phys. Lett.* **1985**, *118*, 263.
- (18) Klenerman, D.; Smith, I. W. M. *J. Chem. Soc., Faraday Trans. 2* **1987**, *83*, 229.
- (19) Varandas, A. J. C.; Yu, H. G. *Mol. Phys.* **1997**, *91*, 301.
- (20) Yu, H. G.; Varandas, A. J. C. *J. Chem. Soc., Faraday Trans.* **1997**, *93*, 2651.
- (21) Szychman, H.; Baer, M.; Varandas, A. J. C. *J. Phys. Chem.* **1997**, *101*, 8817.
- (22) Varandas, A. J. C. *Adv. Chem. Phys.* **1988**, *74*, 255.
- (23) Baulch, D. L.; Cox, R. A.; Crutzen, P. J.; Hampson Jr., R. F.; Kerr, J. A.; Troe, J.; Watson, R. T. *J. Phys. Chem. Ref. Data* **1982**, *11*, 327.
- (24) Szychman, H.; Baer, M. *Chem. Phys. Lett.* **1995**, *242*, 285.
- (25) Szychman, H.; Baer, M. *J. Chem. Phys.* **1996**, *105*, 10380.
- (26) Varandas, A. J. C. *Chem. Phys. Lett.* **1994**, *225*, 18.
- (27) Varandas, A. J. C.; Marques, J. M. C. *J. Chem. Phys.* **1994**, *100*, 1908.
- (28) Kumar, S.; Sathyamurthy, N.; Ramaswamy, R. *J. Chem. Phys.* **1995**, *103*, 6021.
- (29) Ben-Nun, M.; Levine, R. D. *J. Chem. Phys.* **1996**, *105*, 8136.
- (30) Guo, Y.; Thompson, D. L.; Sewell, T. D. *J. Chem. Phys.* **1996**, *104*, 576.
- (31) Lim, K. F. *J. Chem. Soc., Faraday Trans.* **1997**, *93*, 669.
- (32) Marks, A. J. *J. Chem. Phys.* **1998**, *108*, 1438.
- (33) Varandas, A. J. C.; Pais, A. A. C. C. *Theoretical and Computational Models for Organic Chemistry*; Formosinho, S. J.; Czismadia, I. G.; Arnaut, L. G. Eds.; Kluwer: Dordrecht; 1991; p 55.
- (34) Bačić, Z.; Light, J. C. *Annu. Rev. Phys. Chem.* **1989**, *40*, 469.
- (35) Tennyson, J.; Sutcliffe, B. T. *J. Chem. Phys.* **1982**, *77*, 4061.
- (36) Szychman, H.; Varandas, A. J. C.; Baer, M. *J. Chem. Phys.* **1995**, *102*, 3474.
- (37) Clary, D. C. *J. Chem. Phys.* **1991**, *95*, 7298.
- (38) Clary, D. C. *Chem. Phys. Lett.* **1992**, *192*, 34.
- (39) Szychman, H.; Baer, M. *J. Chem. Phys.* **1994**, *101*, 2081.
- (40) Neuhauser, D.; Baer, M. *J. Chem. Phys.* **1989**, *90*, 4351.
- (41) Varandas, A. J. C.; Rodrigues, S. P. J. 12th Annual Meeting of the Portuguese Chemical Society, Coimbra, 1991.
- (42) Murrell, J. N.; Carter, S.; Farantos, S. C.; Huxley, P.; Varandas, A. J. C. *Molecular Potential Energy Functions*; Wiley: Chichester, 1984.
- (43) LeRoy, R. L. *J. Chem. Phys.* **1969**, *73*, 4338.
- (44) Zhang, D. H.; Light, J. C. *J. Chem. Phys.* **1996**, *104*, 4544.
- (45) Varandas, A. J. C. *Chem. Phys. Lett.* **1995**, *235*, 111.